imf
Institute of Materials Finishing

Taylor & Francis
Taylor & Francis Group

OPEN ACCESS

Check for updates

Considerations for digitalisation of nickel electroforming

Sudipta Roy ⓘ and Eleni Andreou ⓘ*

Chemical and Process Engineering, University of Strathclyde, Glasgow, UK

ABSTRACT

This paper is a 'follow-on' from a paper previously published in this journal dealing with the laboratory to pilot scaling up approach using Industry 4.0 manufacturing methods. In particular, the paper reports a strategy for developing a model for the electroforming of nickel from a sulphamate electrolyte at laboratory scale which could subsequently provide an educated approach for transferring the process to a larger scale. At the laboratory scale, a rotating disc electrode assembly was used, which is a standard instrument to determine electrochemical parameters. Thereafter, small scale nickel discs were electroplated using this equipment, and a model of this process was developed and validated against those experimental results. These parameters were then used to actually produce electroforms in a prototype, 18 L tank system. Cross-validation between practical experiments and simulations followed which allowed for fine-tuning the model until it was consistently predicting the real process results within an acceptable error. Overall, it was found that a secondary current distribution model could be used for reasonably accurate description for the electroforming process, and could provide a quick virtual tool at a production facility.

Introduction

As the green transition gains momentum, electroforming has received growing interest, particularly because it is seen as an additive manufacturing method. For example, it has been suggested that it can be used to fabricate protective parts for turbine blades in off-shore and on-shore applications.[1] There are about 341,000 wind turbines around the world,[2] and therefore their production needs to be scalable. For scalability and expense control, it is likely that fabrication methods need to be implemented without resorting to the use of specialised design and consulting houses. This would then require in-house modelling involving workers who have a deep understanding of the process and virtual tooling that is required to enable one to predict the shape, size and thickness of an electroformed part.

Electroforming is a specialised process which is used to fabricate structures using electrochemical deposition. Parts are fabricated on a mandrel which gives the desired shape. These parts have to be detached from the substrate, the mandrel, at the end of the deposition which requires them to have low internal stress in order to retain shape and mechanical integrity. Metals such as gold, copper, silver and nickel, of simple or complex geometry, have been fabricated using electroforming with wider uptake in the aerospace sector.[3,4] Nickel electroforming started developing in the late 50s and 60s, and is technically well established.[5] However, the scientific understanding of the process is still in progress[6,7,8] which has resulted in a preference towards conservative and slow methods of manufacturing instead.

This paper is a 'follow-on' from a paper dealing with the laboratory to pilot scaling up approach using Industry 4.0 manufacturing methods which was published in 2021.[9] In this paper we report on the use of modelling strategies for electroforming for the Industry 4.0 digital era which could be adopted for such in-house production facilities. The modelling tool employed is COMSOL Multiphysics, since it is commercially available software, and can be purchased for in-house analysis. While there can be a variety of reasons for digitalisation, ranging from academic curiosity to understanding a process or engineering it, the focus of this work has been to understand the scalability of the electroforming process when it is transferred from the laboratory scale to the industrial scale.[10] The study has also explored what sort of model is valuable and which process parameters are key in scaling up.[11]

In particular, the paper reports a strategy for developing a model for the electroforming of nickel at laboratory scale which could subsequently provide an educated approach for transferring the process to a larger scale. At the lab scale, a rotating disc electrode assembly was used, which is standard for determining electrochemical parameters. Thereafter, small scale nickel discs were electroplated using this equipment, and a model of this process was developed and validated against those experimental results. This same model was then employed to simulate a scaled-up process and predict the real process operating parameters which would produce a scaled-up disc geometry of a target thickness. These parameters were then used to produce electroforms in a prototype, 18 L tank system. The electroformed scaled-up parts were verified against the modelling results to assess the robustness of the developed model. Continuous cross-validation between practical experiments and simulations followed which allowed for fine-tuning the model until it was consistently predicting the real process results within an acceptable error. Based on this, some outcomes of digitalised manufacturing have been attempted.

Modelling strategy

In order to have a reliable industrial implementation of a process, first, we need to answer what kind of a model is needed. Within the academic literature, models of a high degree of complexity are usually encountered[12–15] – for example, analysis of agitation which is described by complex fluid flow[14] or reaction mechanisms which have been proposed for nickel,[13] or new ideas on the growth of dendrites,[16] etc. Many of these aspects are not relevant in industry; for example, in practice, dendrites are typically being removed from the final product as a standard post-processing step. On the other hand, if the local deposition current could be changed to bring about a change in shape, this could provide flexibility in production. In addition to these considerations, digital analyses should be achievable within reasonable computation times and/or should not require high-grade computation facilities, which may not be available at a production site. In this regard, it is important to strategise modelling tools to benefit production.

The modelling strategy used in this work is to determine if secondary current distribution can be used to predict the thickness of a scaled-up form, based on pre-determined laboratory scale parameters. The need for this stemmed from the fact that, although there is a built-in materials library in COMSOL, this is not relevant to nickel electroforming. Much of the library is based on copper deposition from acid solutions.[3] This is very different from a nickel electroforming bath, which contains $Ni(NH_2SO_3)_2$ (nickel sulphamate), with small amounts of $NiCl_2$ (nickel chloride) and H_3BO_3 (boric acid) as buffer. Copper is relatively noble, and parasitic reactions such as H_2 evolution are absent. Additionally, the kinetics of copper reduction are fast, whereas nickel's are slow. These differences mean that using the standard library of kinetics in COMSOL will return incorrect results, something that the project's industrial partners had experienced extensively while trying to simulate their in-house process by using inbuilt library data instead of nickel ones. Therefore, the first step for any industrial implementation of modelling capability is to obtain a set of parameters for the model relevant to the system being simulated each time. In this work, the first step was, indeed, to obtain relevant parameters for the specific nickel electroforming system which was being studied. The parameters are displayed in Table 1. The methodology for determining these parameters is detailed elsewhere,[10] but briefly described in the Experimental section below.

The second criterion for strategy development is to query 'what can be achieved using a model'. For electrodeposition, one can assume primary (PCD), secondary (SCD) or tertiary

current distribution (TCD) physics, which are all available in COMSOL. PCD results are more useful for fabricating a reactor or adding thieves/masks where existing reactors are being used for plating systems that are kinetically fast, such as copper deposition. Using primary current distribution can provide useful insights into the effects of reactor configuration, electrode size and placement, as well as the ionic conductivity of the system.

SCD studies include the effect of reaction kinetics in addition to primary effects and are more relevant to nickel electroforming. Electroforming electrolytes of nickel exhibit high over-potentials for cathodic deposition, and therefore the assumption of SCD physics is more suitable. If one wishes to change the deposit shape, usually local current distribution can be changed by using thieves and/or masks (in both primary and secondary cases), and the extent of their influence can be constrained by the speed of reaction.

The third level, tertiary current distribution, is mostly used to develop a more accurate result, and includes a full set of the ionic species existing in the electrolyte, including water species, dissolved oxygen, as well as all the active species that can participate in the electrochemical reactions occurring throughout the process. In addition, COMSOL allows one to couple this with fluid flow descriptors, using the computational fluid dynamics (CFD) module, and obtain a more accurate solution. However, for many electroplating and electroforming processes a full understanding of electrolyte speciation,[8] role of additives and their reactions, as well as complex fluid flow in large tanks constrain accuracy. Secondary current distribution, therefore, may provide information and insights which have a similar degree of accuracy to that offered by tertiary current analysis.

COMSOL Multiphysics allows one to solve the Laplace's equation

$$\nabla^2 \Phi = 0 \qquad (1)$$

where $\nabla = i\dfrac{d}{dx} + j\dfrac{d}{dy} + k\dfrac{d}{dz}$ and Φ is the local potential gradient in x, y and z directions. The secondary current distribution includes nickel reduction and dissolution at the cathode and anode using Butler–Volmer kinetics

$$i_{loc,m} = i_{0,m}\left(e^{\frac{\alpha_{a,m}F\eta_m}{RT}} - e^{\frac{-\alpha_{c,m}F\eta_m}{RT}}\right) \qquad (2)$$

where the subscript 'loc' denotes the 'local' current close to the metal surface 'm', α is the transfer coefficient, i_0 is the exchange current density, η is the electrode overpotential, R is the gas constant and T is the temperature. Although it is generally accepted that nickel deposition can occur

Table 1. Physical, chemical and electrochemical parameters for nickel deposition from nickel sulphamate electrolytes.

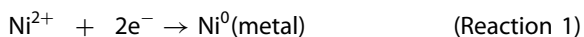|	Parameter	Model	Comments
Electrolyte	Temperature	323 K	User defined (50°C)
	Electrolyte conductivity	0.9165 S/dm	From Experimental Data
Electrodes	Dissolving-depositing species	$Mr_{Ni} = 0.05869$ kg/mol $\rho = 8.908$ kg/L	From literature
	Number of participating electrons	n = 2	$Ni \rightarrow Ni^{2+} + 2e^-$
	Stoichiometric coefficients for dissolving-depositing species	1	$Ni \rightarrow Ni^{2+} + 2e^-$
	Equilibrium potential	$E_{eq} = -0.52$ V	Reversible Potential from Experimental Data
	Exchange current density	$i_{0,m} = 0.42$ A/dm^2	From Experimental Data
	Anodic transfer coefficient	$\alpha_{a,m} = 1.806$	From Experimental Data
	Cathodic transfer coefficient	$\alpha_{c,m} = 0.194$	From Experimental Data
	Limiting Current Density	$i_{lim,m} = 208.138$ A/dm^2	From Experimental Data
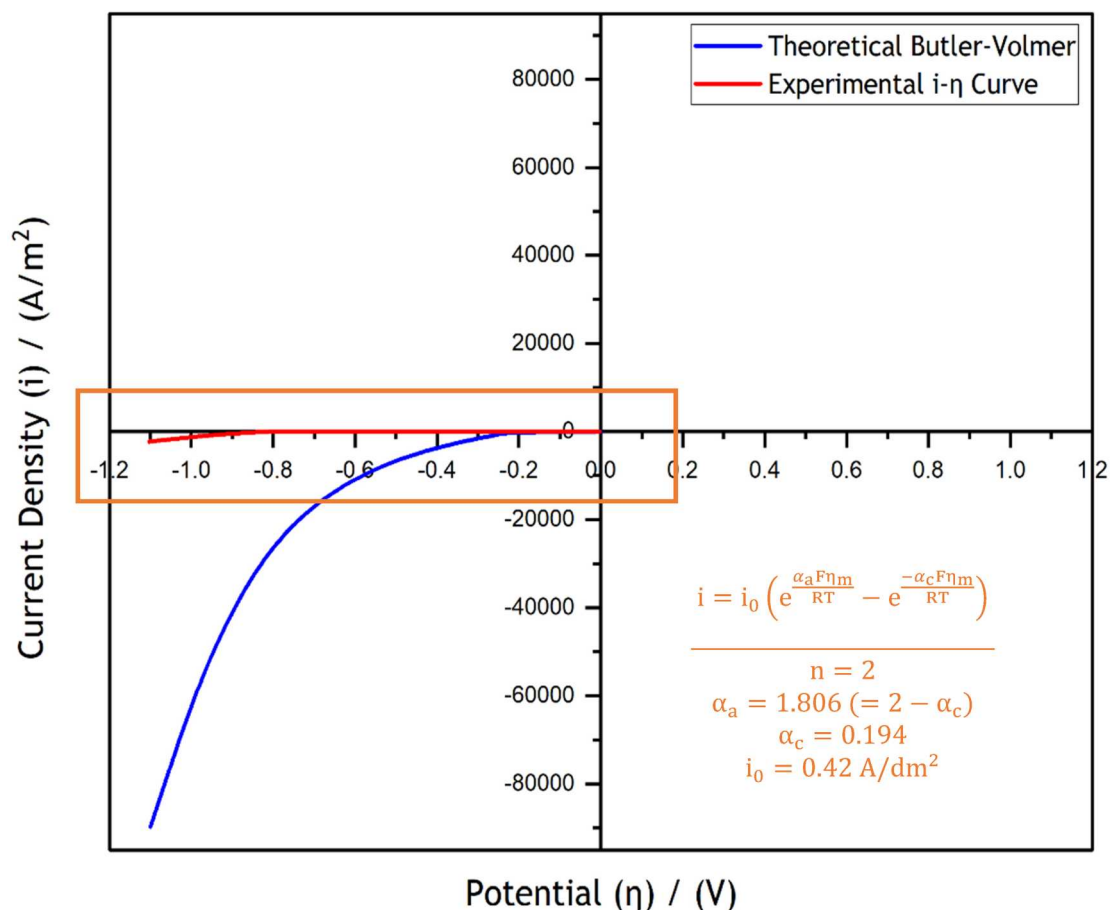
Figure 1. Experimentally recorded and computed polarisation data for nickel deposition from a sulphamate electrolyte at 50°C.

through multiple steps, for COMSOL programming it is sufficient to consider the overall electrochemical nickel reduction or dissolution, i.e.

$$Ni^{2+} + 2e^- \rightarrow Ni^0(metal) \qquad \text{(Reaction 1)}$$

as long as appropriate kinetic parameters are used.

As mentioned, relevant kinetic data for modelling require the collection of current–potential data determined through experimental polarisation measurements. COMSOL expresses this need in the form of overpotentials at the electrode–electrolyte interface in equ. 3:

$$\eta_m = \varphi_s - \varphi_l - E_{eq,m} \qquad (3)$$

where, $E_{eq,m}$ is the reversible potential and φ with subscripts 's' and 'l' are the electrode side and solution side potentials, respectively.

The problem with using equation (3) arises from nickel deposition data, which is shown in Figure 1. The red line is the experimentally gathered current–potential data, and the blue line is that calculated from the data provided by the COMSOL library. The figure shows that there is no clear identifiable reversible potential, as would be expected for sluggish kinetics. COMSOL library provides a nickel reversible potential of −0.26 V, presumably based on thermodynamic data, which does not replicate in any way the experimental current potential data. In addition, the polarisation data for experimental nickel deposition is not exponential, as would be needed for fitting equation (3). In addition, one would need to focus in on the region where the Butler–Volmer equation is to be fitted so that the parameters represent the region of interest.

To circumvent these issues, at first a realistic reversible overpotential needs to be chosen, which was set to −0.52 V. Thereafter, the authors focused on the current–potential regime which was used in practice (denoted by the outlined box in the figure) to obtain kinetic parameters, i_0, α_c and α_a. It is important to understand that these parameters are not independent – since the choice of reversible potential fixes the other three parameters. The methodology adopted for data collection, data fitting, and interpretation is included in previous publications.[10,11] A list of physical and electrochemical parameters used for COMSOL computations are also included in Table 1.

Experimental

Experimentally, in the laboratory, a rotating disc electrode was used to collect current/potential data. The applied current was between 2 and 5 ASD (20–50 mA cm^{-2}) and the temperature was maintained at 50°C, as would be done in industry. An SCE reference electrode was used. Electrode holders were manufactured in-house to replicate stainless steel cathodes (since the mandrel was stainless steel 316), and industrial grade nickel was obtained from suppliers and connected using a titanium rod. A closer view of the anode, cathode holder, and the assembled rotating disc is shown in Figure 2. The electrochemically active surface area of the rotating disc electrode shown in Figure 2(b) was 12 mm in diameter and rotated at 1400 rev min^{-1} to eliminate any mass transfer effects. Deposits of 0.24 mm were electroplated up, and then detached from the electrode surface. The separation of the deposits from the mandrel was easily achieved by
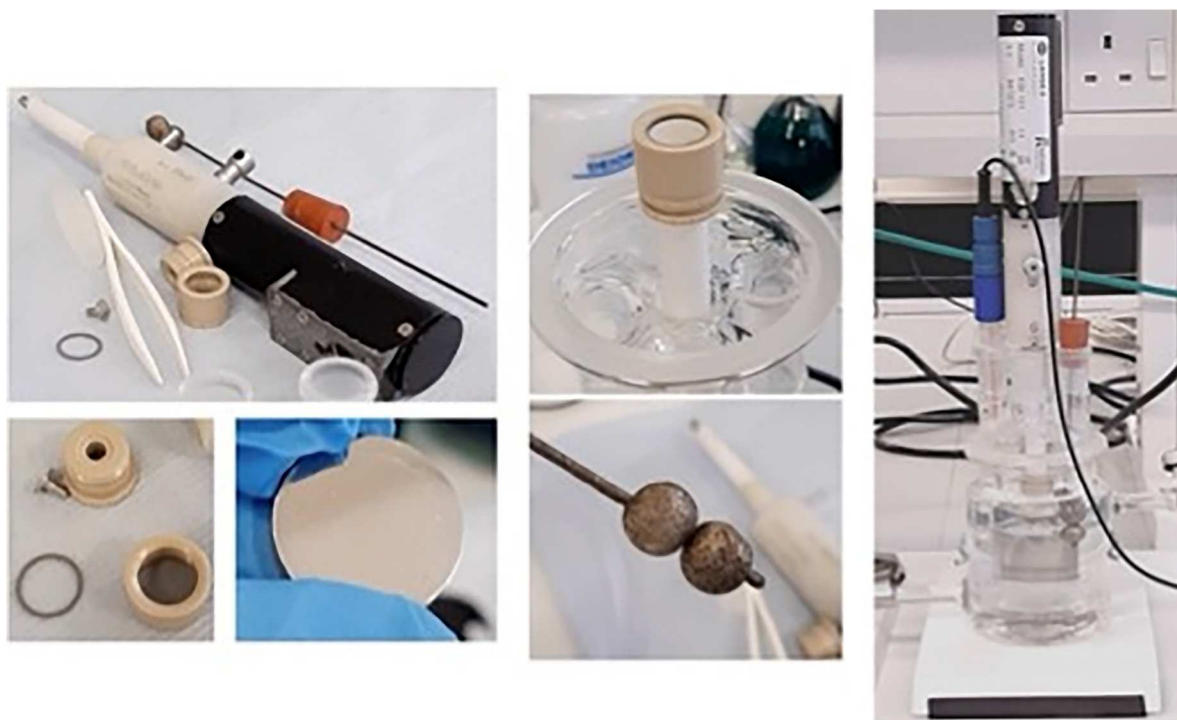
Figure 2. The apparatus used in the laboratory for collection of nickel reduction data. (a) The rotating shaft, anode and cathode holder, (b) a closer view of the cathode holder to ensure exact placement in the cell, (c) cathode holder, (d) stainless steel disc, (e) nickel pellet anodes screwed onto a titanium rod and (f) the cell assembly. The same system was also used to obtain electroformed nickel and modelled using COMSOL.

just pulling them off from the mandrel surface. No tools were required to retrieve the deposits owing to the presence of Nimac 89 UNW wetting agent in the electrolyte which would not allow the deposited material to irreversibly attach on the mandrel.

The scaled-up system was a bespoke piloting tank, which is shown in Figure 3(a). The mandrel is shown (covered with a dark blue tape) in Figure 3(a), and the bottom of the mandrel was exposed so that it formed a large disc. The filled capacity of the tank was 18 L, with extra volume to accommodate, heaters, busbars, a titanium anode basket, an eductor and a

recirculating pump with a filter. This allowed the authors to mimic the conditions used in industry, and verify if the modelling strategy was useful. The tank system has a very different geometry as compared to the electrochemical cell, which is another challenge.

Outcomes

Figure 4(a, b) shows the nickel electroforms obtained using the lab scale and tank scale systems. Interestingly the lab scale electroform shown in Figure 4(a) shows the nodules
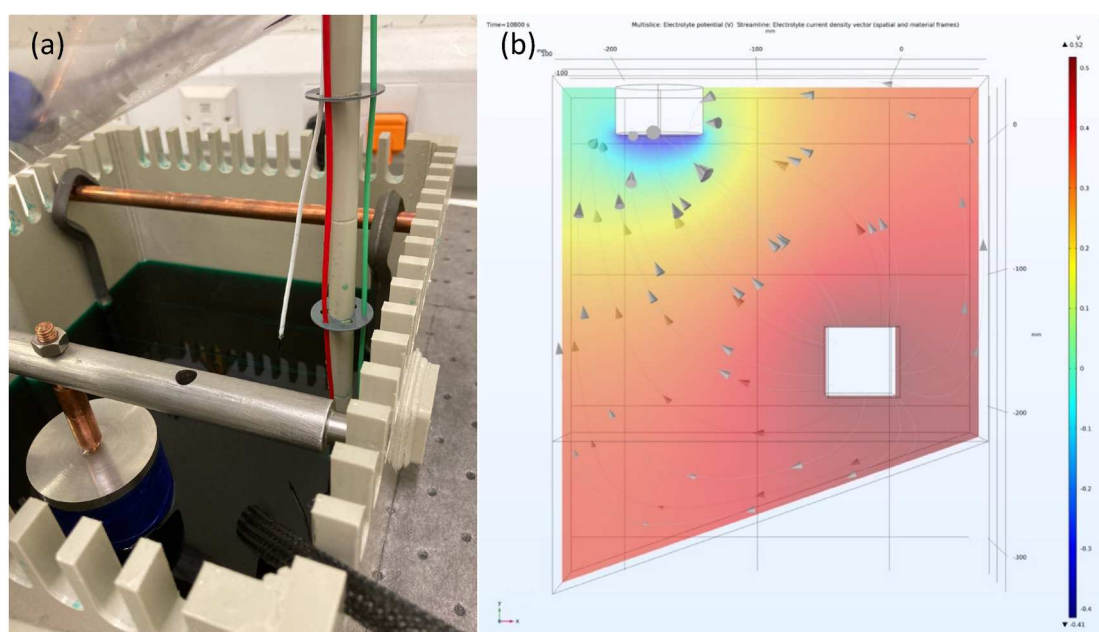

Figure 3. A view of (a) the tank, and (b) its translation to the COMSOL space. The COMSOL 'red' region denotes higher potential near the anode, and lower 'cathodic' potential occur around the cathode. The arrows denote the current lines and direction from the anode to the cathode. The full-size version of Figure 3-b is provided in the Supplementary Materials section.
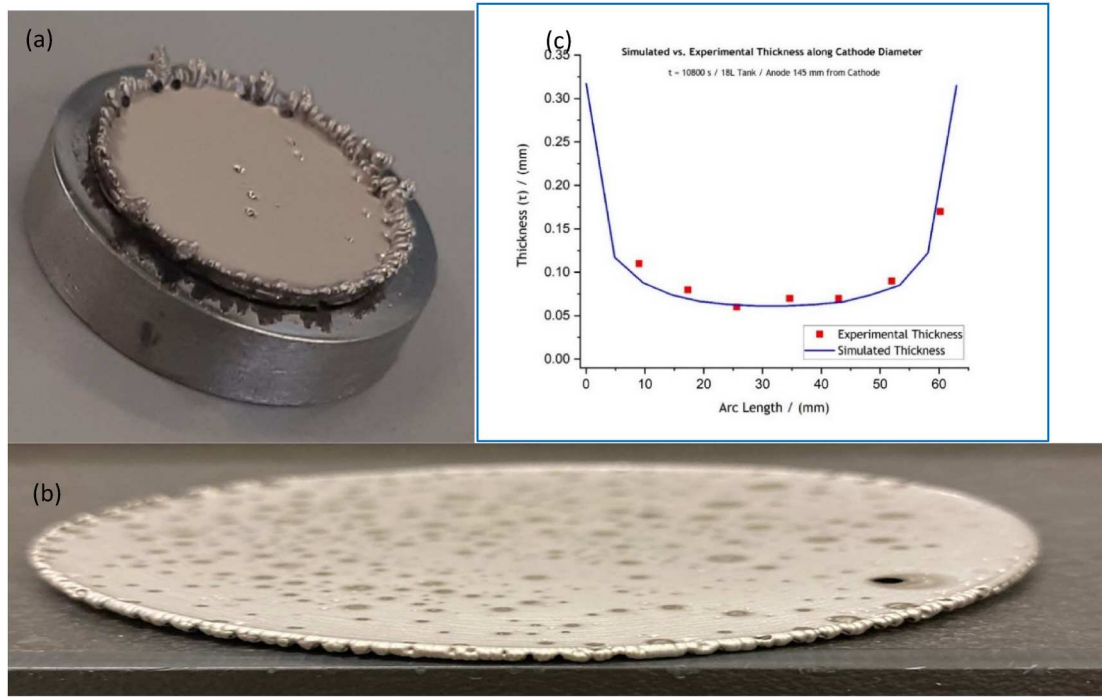
Figure 4. Electroforms used for validation of models (a) nickel deposit on stainless steel rotating disc cathode (d = 12 mm), (b) nickel deposited on steel mandrel in the tank (D = 65 mm) and (c) thickness of electroformed disc at different positions as determined from model computations (blue line) and experimental data (red squares).

(or dendrites) of nickel at the edges which are often observed in industrial scale manufacturing. The methodology for computing deposit thickness and its verification has been published elsewhere[11,12] and therefore is not repeated here.

The scaled-up system also provided coherent electroforms, although additional issues arose from gas bubbles sticking to the mandrel surface, as shown in Figure 4(b). For verification, the electroform shown in Figure 4(b) was sectioned and measured for thickness using scanning electron microscopy, and the outcome of the thickness measurements compared against those predicted by COMSOL computations is shown in Figure 4(c). The figure shows that the model predicts the thickness of the electroformed nickel disc with good agreement. Although here only one set of results is reported, these findings have been replicated a number of times and at different currents and deposition times[11,12,17].

An important result from this analysis is that models using secondary current distribution may provide an adequate basis for in-house industrial implementation. Generally, models are assessed on their complexity and accuracy; the lower the complexity and higher the accuracy, the better is the model. Using COMSOL, both secondary and tertiary current distributions can be carried out, and a user may feel tempted to only use tertiary current solutions. However, the TCD results, even though more insightful, might not be so much more useful to industry, compared to SCD ones, to justify the use of a much more complicated TCD model over a SCD one. To support this statement, a brief comparison of SCD vs TCD modelling results is presented here.

While both PCD and SCD models assume uniform ionic concentration in the electrolyte, TCD models take into account concentration gradients in the electrolytic volume, alongside solution resistance (PCD) and kinetic (SCD) contributions. For this purpose, the Nernst-Planck equation

(equation (4)) is solved for each chemical species (i) present in the electrolyte, describing each one's mass transport through diffusion, migration and convection.

$$N_i = -D_i \nabla c_i - z_i v_{m,i} F c_i \nabla \varphi_l + c_i u \qquad (4)$$

where, N_i is the flux of species i (mol/m$^2 \cdot$ s), D_i the species diffusion coefficient (m^2/s), c_i the concentration of the ion of species i (mol/m^3), z_i the species charge number, $v_{m,i}$(s · mol/kg) the species mobility and u(m/s) the field velocity vector.

Briefly, the TCD interface solves for the electrolyte potential (φ_l), the electrode potential (φ_s) and the species concentrations (c_i). Equation (5) describes the electrode boundaries,

$$i_s = -\sigma_s \nabla \varphi_s \qquad (5)$$

where, i_s is the current density vector at the electrode and σ_s is the electrolyte conductivity close to the electrode surface.

Equation (6) describes the electrolyte domain, while equation (7) constitutes the typical Butler–Volmer model expression for current density locally, at the electrode–electrolyte interface. Importantly, the reference concentration (c_{ref}) should remain the same for all species involved in a reaction to ensure that, at equilibrium, the overpotential satisfies equation (3).

$$i_i = -F\left(\nabla \sum_i z_i D_i c_i\right) - F^2 \nabla \varphi_l \sum_i z_i^2 v_{m,i} c_i \qquad (6)$$

$$i_{loc,m} = i_{0,m}\left(\frac{c_{Red}}{c_{ref}} e^{\frac{\alpha_{a,m} F \eta_m}{RT}} - \frac{c_{Ox}}{c_{Ref}} e^{\frac{-\alpha_{c,m} F \eta_m}{RT}}\right) \qquad (7)$$

The last task in the development of the TCD model was to identify the ion species involved in the electrochemical system. As mentioned, only nickel deposition was assumed to occur on the cathode surface according to (Reaction 2),
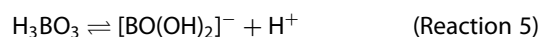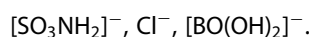
being the source of one ion species, Ni^{2+}.

$$Ni^{2+} + 2e^- \rightarrow Ni \qquad \text{(Reaction 2)}$$

Considering the electrolyte components mentioned earlier, three more ion species were identified (Reactions 3–5):

Table 2. Model input parameters describing each chemical ionic species involved.

Species	Initial concentration ($c_{0,i}$ − mol/m^3)	Charge number (z_i)	Diffusion coefficient ($D_{c,i}$ − m^2/s)	Reference
Ni^{2+}	1632.49519	+2	6.61×10^{-10}	[14]
[SO$_3$NH$_2$]$^-$	3152.1554	−1	5.23×10^{-10}	[15]
Cl$^-$	112.834978	−1	2.030×10^{-9}	[16]
[BO(OH)$_2$]$^-$	566.06825	−1	10.996×10^{-9}	[17]
H$^+$	Automatically Calculated for Electroneutrality	+1	9.3×10^{-9}	Software
OH$^-$	Automatically Calculated for Electroneutrality	−1	5.3×10^{-9}	Software

[SO$_3$NH$_2$]$^-$, Cl$^-$, [BO(OH)$_2$]$^-$.

$$Ni(SO_3NH_2)_2 \rightleftharpoons Ni^{2+} + 2[SO_3NH_2]^- \qquad \text{(Reaction 3)}$$

$$NiCl_2 \rightleftharpoons Ni^{2+} + 2Cl^- \qquad \text{(Reaction 4)}$$

$$H_3BO_3 \rightleftharpoons [BO(OH)_2]^- + H^+ \qquad \text{(Reaction 5)}$$

Since an aqueous electrolytic solution is used, water-based electroneutrality is assumed with two more species deriving from the dissociation of water (Reaction 6): H$^+$ and OH$^-$.

$$H_2O \rightleftharpoons H^+ + OH^- \qquad \text{(Reaction 6)}$$

For the development of the model, the dissociation of every electrolyte component was assumed to be happening instantaneously and was complete (i.e. 100% dissociation). Therefore, all species were assumed to be present in their ionic form and no equilibration reactions were taken into consideration in the electrolytic volume. The input parameters
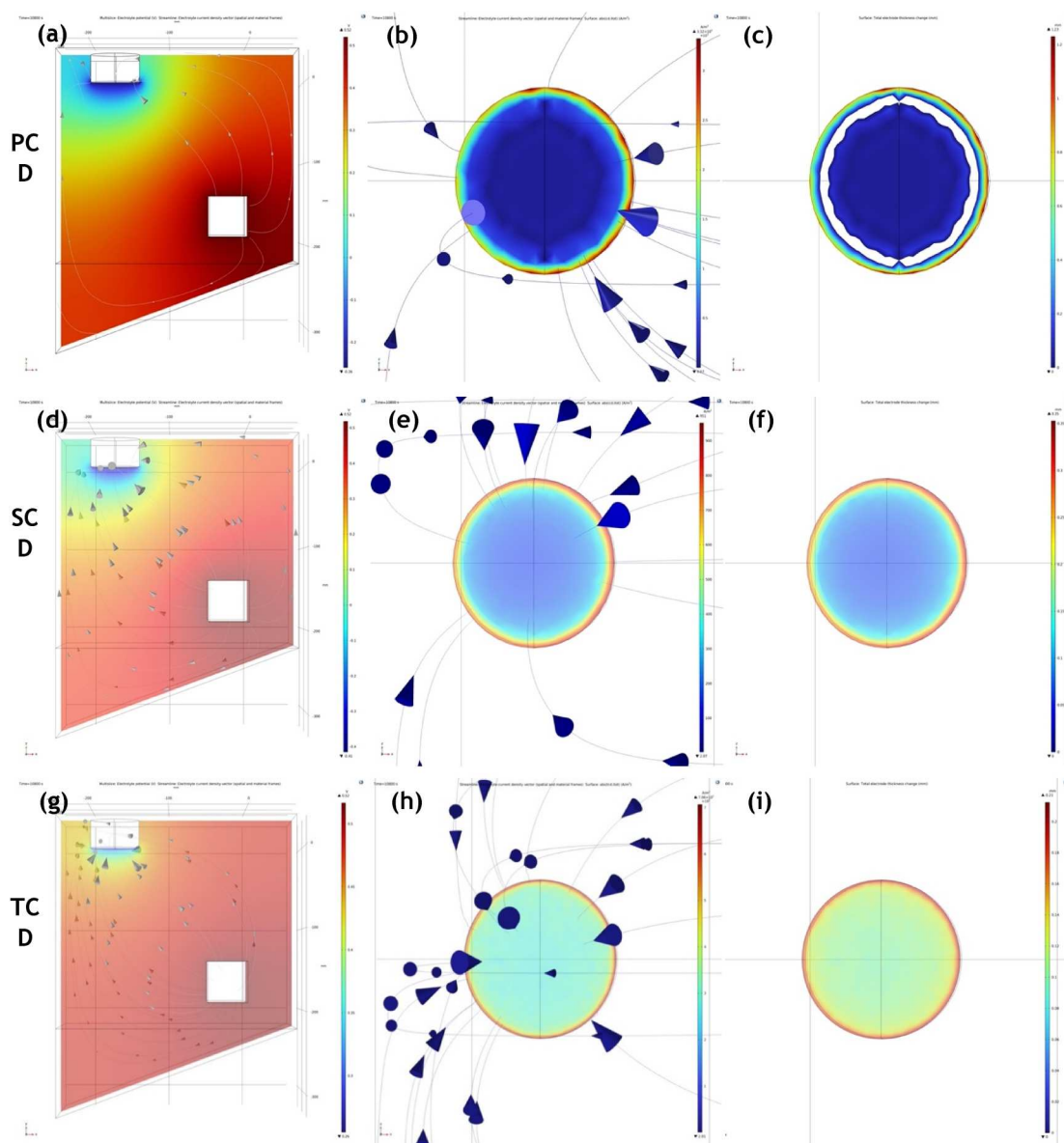

Figure 5. 3-D representation of (a) the potential distribution in the electrolyte, (b) the current distribution at the cathode surface and (c) the thickness distribution at the cathode surface for the PCD scaled-up disc model. 3-D representation of (d) the potential distribution in the electrolyte, (e) the current distribution at the cathode surface and (f) the thickness distribution at the cathode surface for the SCD scaled-up disc model. 3-D representation of (g) the potential distribution in the electrolyte, (h) the current distribution at the cathode surface and (i) the thickness distribution at the cathode surface for the TCD scaled-up disc model when considering all ionic species in the electrolyte. The results simulate potential, current and thickness distributions for deposition processes conducted at −1 A (16A/dm^2) and −2.5 V, for 10800 s at 50°C. The full-size version of each individual figure is provided in the Supplementary Materials section.

required by the software to describe each one of the ionic species involved are provided in Table 2.

Figure 5 provides a complete comparison of the potential distribution in the electrolyte, as well as the current and thickness distributions at the cathode surface for PCD, SCD and TCD models of the scaled-up disc model. By a comparison of Figures 5(a, d and g) it can be observed that the potential range remains almost unaffected between the PCD (−0.26 V ↔ 0.52 V) and SCD (−0.41 V ↔ 0.48 V) conditions. On the other hand, the corresponding range for the TCD model appears more limited (0.2 V ↔ 0.52 V) compared to the two other models. For all three models, the maximum potential value coincides with the set equilibrium potential ($E_{eq} = -0.52\ V$) and it appears in the electrolyte volume close to the anode surface.

The density of the current streamlines is predicted to be the most amplified for the TCD model (Figure 5h). However, even though the SCD model presents the more balanced behaviour (Figure 5e), the disorder of the PCD model is significantly increased (Figure 5b), with current streamlines not even reaching part of the cathode surface (Figure 5a). Consequently, the PCD model suggests that a surface around the leading edge is not even deposited (white area in Figure 5c). The different current distributions at the cathode surface for the PCD, SCD and TCD models are, consequently, depicted in the thickness distributions at the cathode surface (Figure 5c, f & i).

The comparison, between the simulated and experimentally achieved thicknesses, among PCD, SCD and TCD models of the electroforming of a scaled-up disc, is provided in Figure 6. Here, it is shown that the SCD model is validated by experimental results in the larger scale. The PCD model underpredicts the thickness while also suggesting unreasonably high current values at the leading edge, in line with the corresponding simulated disorder of the current distribution (Figure 5b). The TCD model overpredicts the deposit thickness.

Here a comparison between the thickness profile suggested by a 4-species TCD model (magenta line) versus a 6-species TCD model (green line) is also provided. The 4-species TCD model assumed the activity of only Ni^{2+}, $[BO(OH)_2]^-$, H^+ and OH^-, while the 6-species one assumed that all ionic species in Table 2 are active in the electrolyte.

From the comparison it is clear that the latter returns more uniform results and is qualitatively closer to the experimental ones (red data points). However, both TCD models' results do not deviate significantly in terms of the simulated average thickness (~ 0.12 mm). These results show that TCD models are sensitive to species selected, even when they are present in small (almost negligible/undetectable) amounts in the electrolytic solution. This poses one of the main challenges in TCD since many plating solutions do not have well understood speciation.

One important difference, the computation time for the case of the 4-species TCD model exceeded 17 h while in the case of the 6-species TCD model was more than 2 times slower (over 34 h). In any case, the results presented here suggest that SCD models may be sufficient to predict deposit thickness. TCD models may provide additional (different) information, but they need longer to converge. This may mean that SCD models for high volume metal deposition may be a reasonable approach when nearly real time solutions are needed, such as current efficiencies
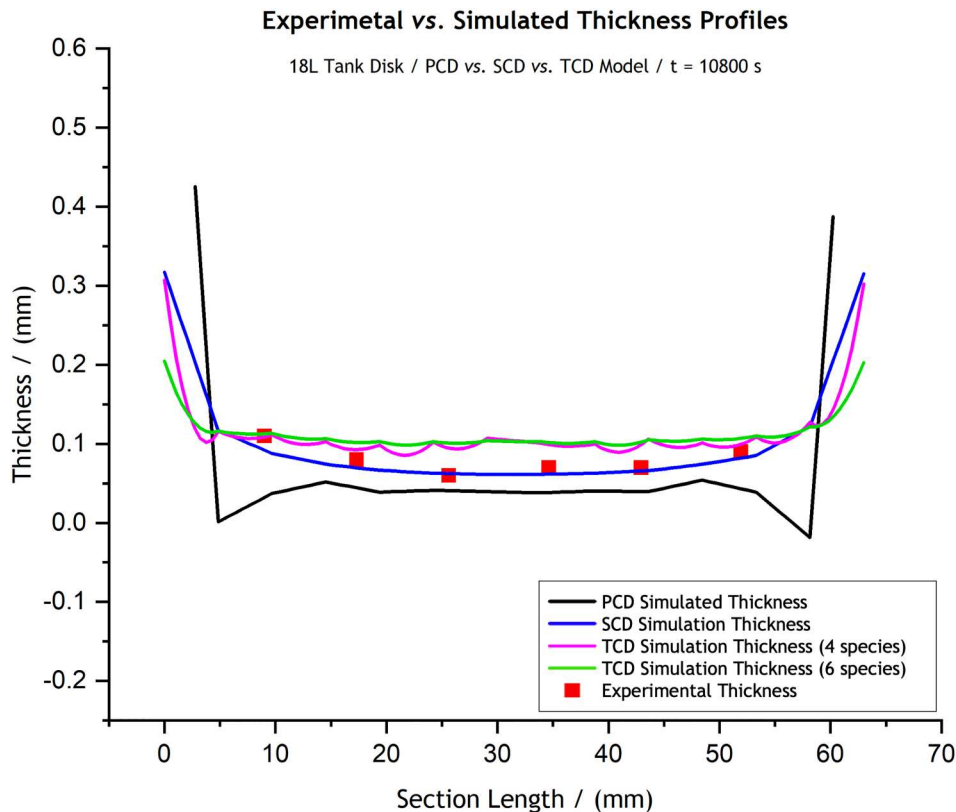

Figure 6. Comparative graphs of the experimentally achieved (red data points) and the simulated thickness profiles by the PCD (black line), SCD (blue line), TCD assuming four ionic species (magenta line) and TCD assuming six ionic species (green line) scaled-up disc setup models. The scaled-up disc deposit was produced at −2.5 V and −1 A, for 10800s at 50°C. Note that the section length of the x-axis is, essentially, the radius of the deposits (D = 65 mm).

or potential currents etc. Additionally, as is also the case for the laboratory-scale RDE models, the computation time for the large-scale, 6-species, TCD model was more than 408 times slower compared to the corresponding SCD one which converged after 300 s. There has been a prior attempt to use CFD-combined with Ni deposition from sulphamate using COMSOL[18]. However, the researchers used COMSOL library values for electrodeposition (as discussed earlier in the modelling strategy section) and not nickel, which makes it difficult to compare results from the current study against theirs.

Conclusions

This work examined the scalability of secondary current distribution from lab scale to industrial scale electroforming. For this, experimental data was gathered in a laboratory, which provided the parameters for the process. Thereafter, electroforms were fabricated using the laboratory scale system. The system was then used to fabricate electroforms using a scaled-up 18 L plating tank. In parallel, modelling was carried out to predict the local thickness of the electroformed parts in the tank. The thickness of the part at different locations was measured and the model validation was carried out by comparing the two thicknesses. Secondary current distribution analysis was found to provide good prediction for the electroformed part, which may be useful for implementation in a production facility.

Acknowledgements

Disclosure statement

ORCID

Sudipta Roy http://orcid.org/0000-0002-3399-035X
Eleni Andreou http://orcid.org/0000-0003-2973-2697

References

1. R. Herring, K. Dyer, F. Martin and C. Ward: *Renewable Sustainable Energy Rev.*, 2019, **115**, 109382.
2. https://gwec.net/, down-loaded on 27/09/2024
3. S. Watson: *Trans. IMF.*, 1989, **67**(1), 89–94.
4. A. Uriondo, M. Esperon-Miguez and S. Perinpanayagam: *J. Aerospace Eng.*, 2015, **229**(11), 2132–2147.
5. S. Watson. 'Applications of electroforming: a report from the Nickel Development Institute', 1990.
6. S. Roy and E. Andreou: *Curr. Opin. Electrochem.*, 2020, **20**, 108–115.
7. T. A. Green, C. E. Tambe and S. Roy: *J. Electrochem. Soc.*, 2022, **169**, 092510.
8. C. Enowmbi Tambe, T. A. Green and S. Roy: *J. Electrochem. Soc.*, 2024, **171**, 102503. doi:10.1149/1945-7111/ad80d3.
9. E. Andreou and S. Roy: *Trans. IMF.*, 2021, **99**(6), 299–305.
10. E. Andreou and S. Roy: *Front. Chem. Eng.*, 2022, **4**, 755725.
11. E. Andreou and S. Roy: *Digit. Chem. Eng.*, 2024, **12**, 100177. doi:10.1016/j.dche.2024.100177.
12. A. Behagh, A. Fadaei Tehrani, H. SalimiJazi and O. Behagh: *Iran. J. Mater. Sci. Eng.*, 2015, **12**, 20–27.
13. I. Epelboin and R. Wiart: *J. Electrochem. Soc.*, 1971, **118**, 1577–1582.
14. I. Belov, C. Zanella, C. Edström and P. Leisner: *Mater. Design*, 2016, **90**, 693–703.
15. A. M. Behagh, A. R. F. Tehrani, H. R. S. Jazi and S. Z. Chavoshi: *J. Mech. Eng. Sci.*, 2012, **10**, 2306–2314.
16. C. Lupo and D. Schlettwein: *J. Electrochem. Soc.*, 2019, **166**, D3182–D3189.
17. Eleni Andreou, 'Nickel electroforming for large scale applications: process modelling and optimisation', PhD thesis, University of Strathclyde, 2022.
18. H. Zhang, N. Zhang and F. Fang: *J. Manuf. Sci. Eng.*, 2021, **143**(11), 111005.